

Regional patterns of ice-wedge degradation since the mid-20th century across northern Alaska

Gerald V. Frost^{1*}, Matthew J. Macander¹, Donald A. Walker², Martha K. Reynolds², and Anna Liljedahl³

¹ABR, Inc. – Environmental Research and Services, Inc., Fairbanks, AK

²Alaska Geobotany Center, University of Alaska Fairbanks

³Water and Environmental Research Center, University of Alaska Fairbanks

*corresponding author <jfrost@abrinc.com>



Abstract

Ice-wedge polygons are abundant in the continuous permafrost zone of Alaska's North Slope, creating complex microtopography and strong, meter-scale contrasts in hydrologic regime, vegetation, and ground ice conditions. Rapid and dramatic landscape changes have occurred in recent decades in the coastal plain of the eastern North Slope due to thawing of the uppermost portions of ice wedges. Thaw of the wedges results in ground subsidence (thermokarst) and the formation of flooded pits along the polygon margins. Secondary impacts, including thermal degradation of permafrost and spatially-variable flooding and drainage of polygon centers, affect areas well beyond the thermokarst pits themselves. Archives of historical (1948, 1955, 1971, 1977–1985) and modern high-resolution imagery support regional-scale detection of ice-wedge degradation across bioclimatic (north-south) and geomorphic (east-west) gradients spanning the North Slope. To characterize the timing and extent of ice-wedge degradation, we delineated small waterbodies in historical and modern imagery for a network of eleven 43 km² study areas spanning the North Slope, including sites where we collected field data in 2010–2012. We conducted spatial analyses of imagery to delineate waterbodies in color-infrared aerial photography (1979–1985), and modern high-resolution satellite imagery (2009–2012), using an iterative process by which we set a threshold near-infrared reflectance value, and then assessed whether pixels with reflectance values beneath this threshold corresponded to water or land. Spatial analysis of surface water extent indicated increases in the total area occupied by flooded thermokarst pits at 8 of 11 landscapes since circa 1980 (median +10.6%; maximum 77.8%). The 3 landscapes where water extent decreased are all located on the western North Slope; photography from 1948–1955 indicates similar surface water distribution to that present today at these sites. Increases in the extent of thermokarst pits were prevalent on the eolian sand sheet, and eolian silt deposits (yedoma.) Because the ice wedges underlying the North Slope have developed over millennial timescales, the changes observed over the past few decades appear to represent a directional change, rather than a cyclic process whereby local thermokarst is offset by ice aggradation elsewhere. Our results also indicate an intriguing regional pattern of ice-wedge degradation, in that thermokarst pit development appears to have occurred earlier on alluvio-marine deposits, which are prevalent on the western North Slope. Future work involves remote-sensing and field-based approaches to identify drivers of the changes and regional patterns observed since the mid-20th century.

Introduction & Methods

Numerous reports of ice-wedge thermokarst have emerged over the last decade from across the Pan-Arctic, including the Alaska North Slope (Jorgenson et al. 2006, Reynolds et al. 2014), the Canadian High Arctic (V. Romanovsky, unpub. data), and the forest-tundra ecotone in northeast Siberia (Frost and Epstein 2014) (Figs. 1, 2). Here we evaluate regional patterns of ice-wedge degradation across the Alaska North Slope, where ice-wedge polygons are widespread and conspicuous, and for which extensive archives of historical high-resolution photography exist to identify spatio-temporal patterns of landscape change. The study area encompasses three geomorphic environments with differing substrates, landscape histories, and ground ice conditions: (1) alluvio-marine deposits along the Chukchi Sea coast; (2) the eolian sand sheet southeast of the Barrow arch; and (3) ice-rich eolian silt (yedoma) of the northern Brooks Range foothills (Fig. 3).

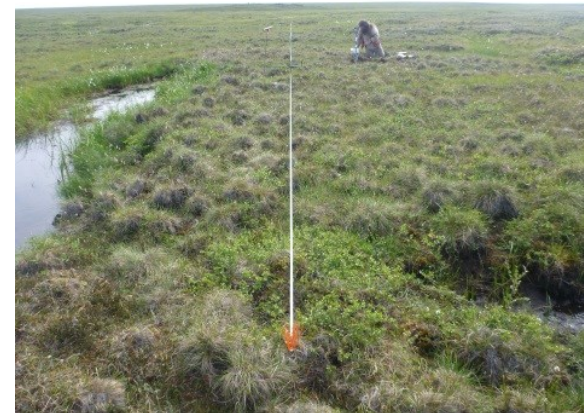


Figure 1. The initiation of thermokarst pits (at left) triggers ground subsidence, vegetation mortality, ponding, and the alteration of flowpaths in adjacent areas leading to spatially-variable wetting and drying. Over time, pits become stabilized by colonizing wetland vegetation and the development of an organic mat.

We quantified the extent of small (< 500 m²) thermokarst pits evident in color-infrared (CIR) photography from the Alaska High Altitude Photography Program (AHAP) (1977–1985), and in modern very-high-resolution satellite imagery (2010–2012) across a network of eleven 43 km² study areas. To distinguish thermokarst pits, we exploited near-infrared (NIR) reflectance values, which are typically lowest for open water and much higher for vegetated land. For this analysis, we focused on old, residual upland landscapes, where ice wedges have developed over long periods of time and where small waterbodies are generally restricted to thermokarst pits. We used 5-m resolution IFSAR DEMs to mask low-lying areas, such as drained lake basins, where there is high inter-annual variability in water level and changes are difficult to interpret. We also referred to older (1948–1955), black & white aerial photography to estimate the extent of thermokarst pits in prior decades.

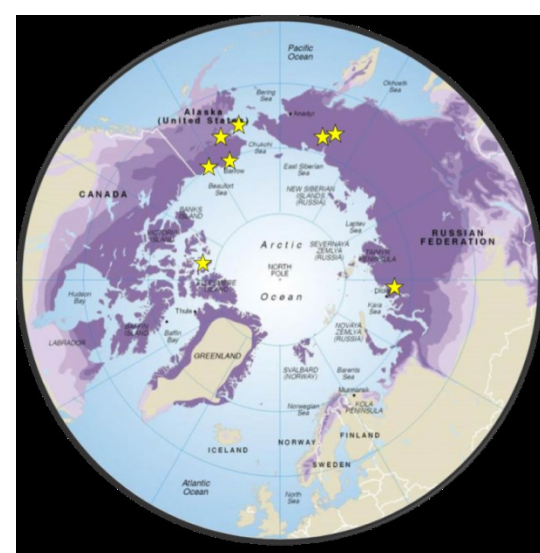


Figure 2. Reports of recent ice-wedge degradation span most of the circumpolar Arctic. From Liljedahl et al. (2013).

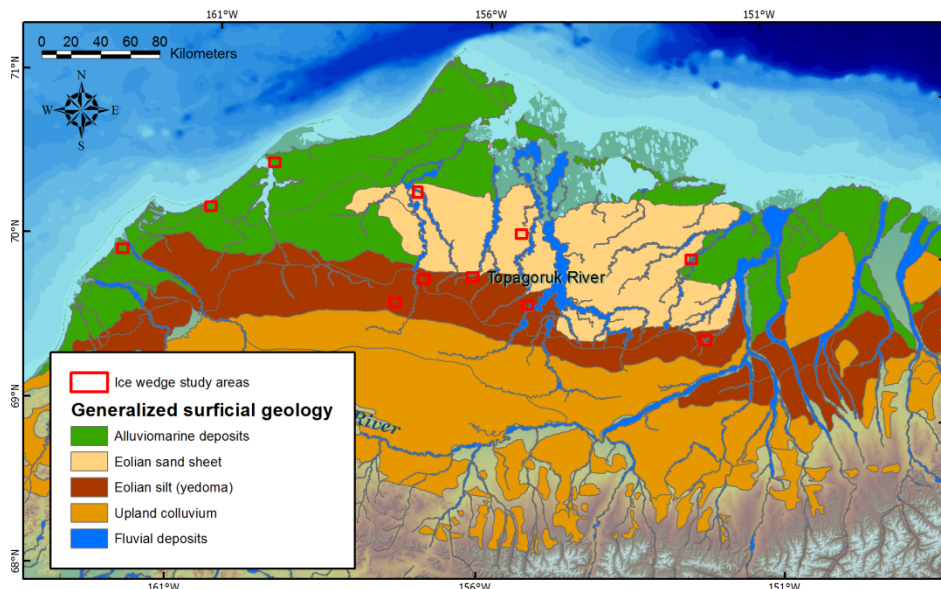


Figure 3. Study sites (red boxes) are distributed in three distinct geomorphic environments: alluvio-marine deposits, the eolian sand sheet, and eolian silt (yedoma) in the foothills. Mapping after Jorgenson and Grunblatt (2013).

Results

Spatio-temporal analysis revealed increases in the total area of flooded thermokarst pits at 8 of 11 study landscapes since ~1980 (Table 1, Figs. 4–7). On a percent basis, change in the cover of flooded pits ranged from -27.3% – +134.6% (median +10.0%). We caution, however, that we were conservative in establishing the thresholds of near-infrared reflectance values used to identify changes in surface water in extent, so actual changes in thermokarst pit area are probably somewhat higher than our results indicate.

Pit extent decreased on 2 of 3 alluvio-marine sites, although moderate increases were observed at one alluvio-marine site. Pit extent increased at all 3 sites on the eolian sand sheet, and at 4 of 5 yedoma sites. The most dramatic changes by far occurred on ice-rich yedoma. Pit extent more than doubled at Kogosukruk River; however, pit extent decreased substantially at one yedoma site (Upper Meade River). A regional pattern is also evident from west to east. Changes in thermokarst pit extent were predominantly negative at the westernmost sites, and there is a sharp rise in recent thermokarst rates moving from west to east across the study area. (Fig. 8).

Table 1. Summary of study area locations, imagery dates, and observed changes in thermokarst pit extent (circa 1980–2010). Negative values are shown in parentheses.

| Study area | Latitude (°N) | Longitude (°E) | AHAP imagery date | Modern imagery date | Total pit area (ha) | | | % change decade ⁻¹ |
|-------------------|---------------|----------------|-------------------|---------------------|---------------------|--------|----------|-------------------------------|
| | | | | | AHAP | Modern | % change | |
| Kugachiak Creek | 70.0 | -162.3 | 16 Jul 1982 | 08 Aug 2010 (GE-1) | 176.3 | 161.5 | (8.4) | (13.6) |
| Ongorakvik River | 70.3 | -160.9 | 02 Aug 1985 | 05 Jul 2012 (WV-2) | 166.6 | 196.7 | 18.1 | 6.5 |
| Wainwright SRRS | 70.6 | -159.8 | 18 Jul 1982 | 08 Jul 2012 (WV-2) | 30.7 | 23.9 | (22.1) | (7.4) |
| Upper Meade River | 69.8 | -157.5 | 16 Jul 1982 | 19 Jul 2009 (GE-1) | 16.6 | 12.1 | (27.3) | (3.1) |
| Atkasuk East | 70.5 | -157.2 | 02 Aug 1985 | 22 Jul 2012 (GE-1) | 0.8 | 0.9 | 11.3 | 4.2 |
| Piksaksak Creek | 70.0 | -157.0 | 16 Jul 1982 | 22 Jul 2012 (GE-1) | 3.8 | 6.1 | 61.0 | 20.3 |
| Topagoruk River | 70.0 | -156.2 | 16 Jul 1982 | 09 Jul 2010 (GE-1) | 12.4 | 13.0 | 4.7 | 1.7 |
| Oumalik River | 70.3 | -155.4 | 16 Jul 1982 | 15 Jul 2009 (GE-1) | 43.3 | 47.6 | 10.0 | 3.7 |
| Titaluk River | 69.8 | -155.2 | 16 Jul 1982 | 25 Jun 2010 (WV-2) | 25.7 | 45.6 | 77.8 | 27.8 |
| Judy Creek | 70.1 | -152.4 | 13 Jul 1979 | 22 Jul 2012 (GE-1) | 5.0 | 7.8 | 55.8 | 16.9 |
| Kogosukruk River | 69.6 | -152.2 | 1 Aug 1977 | 22 Aug 2011 (WV-2) | 7.5 | 17.7 | 134.6 | 39.6 |

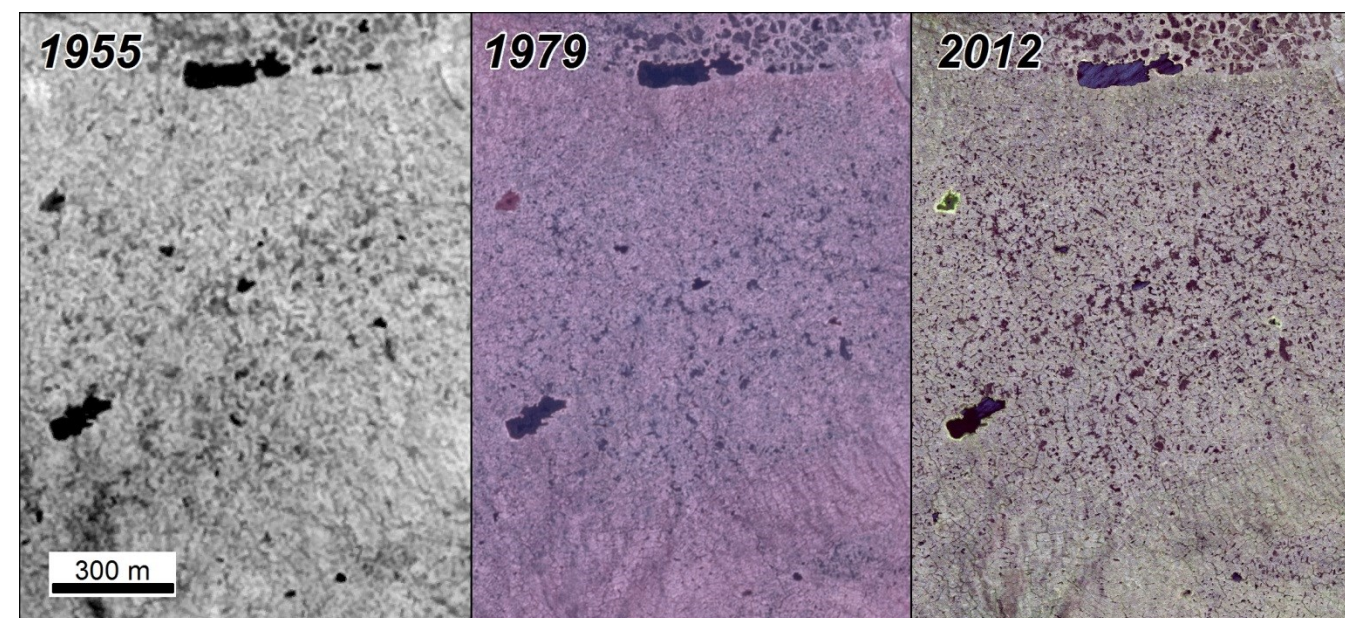


Figure 4. Thermokarst pit evolution at Wainwright study area, 1955–2010. Most of the thermokarst pits present in 2012 were already evident in 1955 imagery. Surface water extent decreased overall at 2 of the 3 westernmost study areas, on alluvio-marine deposits. In contrast to sites further east, thermokarst pits were already widespread along the Chukchi coast by 1955.

Figure 5. Timeline of ice wedge degradation at Oumalik River study area on the eolian sand sheet, 1948–2010. Very few thermokarst pits were evident here in 1948, but the landscape has since become pock-marked with thermokarst pits. Recent changes in pit area, and their overall abundance are quite variable on the sand sheet, perhaps reflecting high variability and ground-ice content; ice content can be very low in sandy substrates.

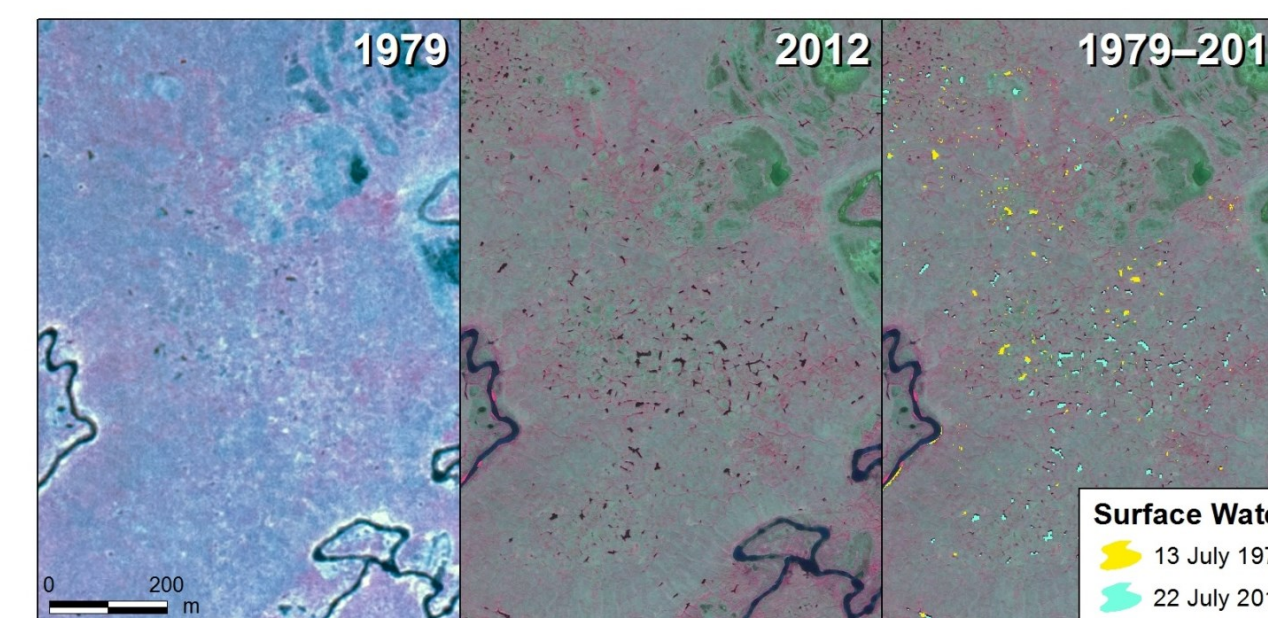
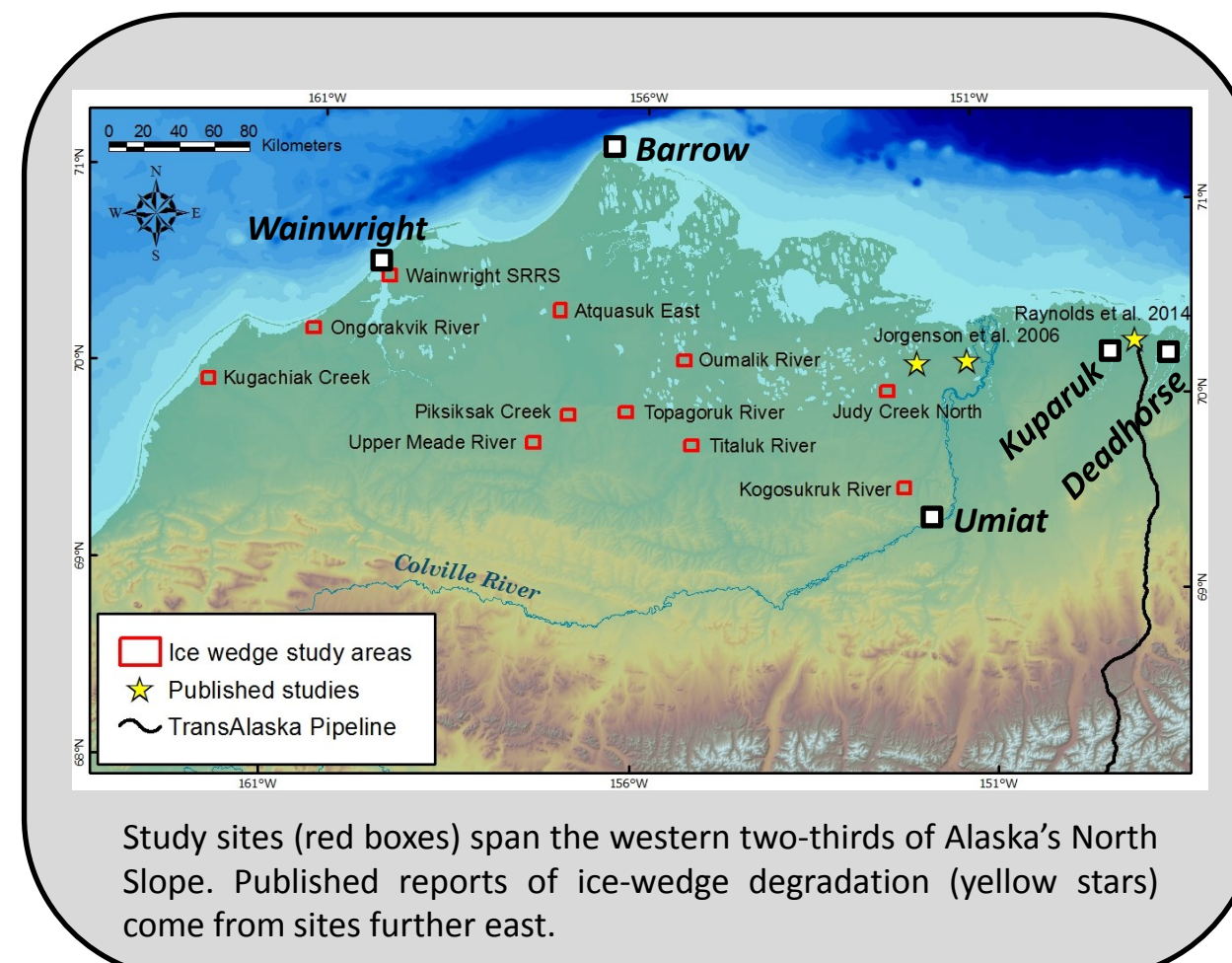


Figure 6. Thermokarst pit development on eolian sand sheet at Judy Creek study area, 1979–2012. The extent of flooded pits increased by 56% at this study area. Note that some of the pits evident in 1979 no longer hold surface water and have been recolonized by vegetation.



Study sites (red boxes) span the western two-thirds of Alaska's North Slope. Published reports of ice-wedge degradation (yellow stars) come from sites further east.

Figure 7. Timeline of ice wedge degradation at Titaluk River study area, in the foothills yedoma belt, 1948–2010. Only a few thermokarst pits are evident in the 1948 photo. Initiation and growth of thermokarst pits accelerated dramatically after 1982. The “yedoma belt” of the Brooks Range foothills is characterized by small Holocene ice wedges overlying very large, Pleistocene-age ice wedges (see Figure 8, above right).

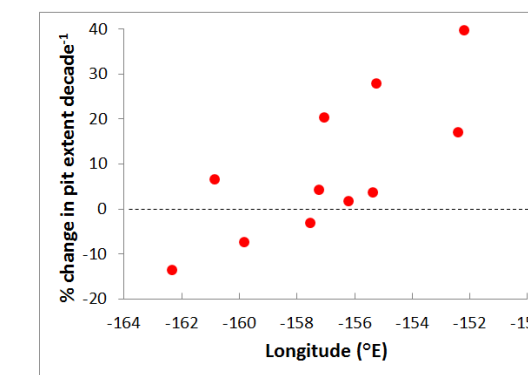


Figure 8. Decadal rates of change in thermokarst pit extent exhibit a regional pattern, with decreasing extent prevalent in the west, and highest rates of increase in the east.



Fig. 9. Field-measured elevations of ground surface and permafrost table along a ~200 m transect spanning newly-developed thermokarst pits (yellow arrows) and remnant high-center polygons near Kogosukruk Creek, in 2009 and 2014. Rapid subsidence is evident at several locations (arrows), and has created new flowpaths for soil water atop the permafrost table.

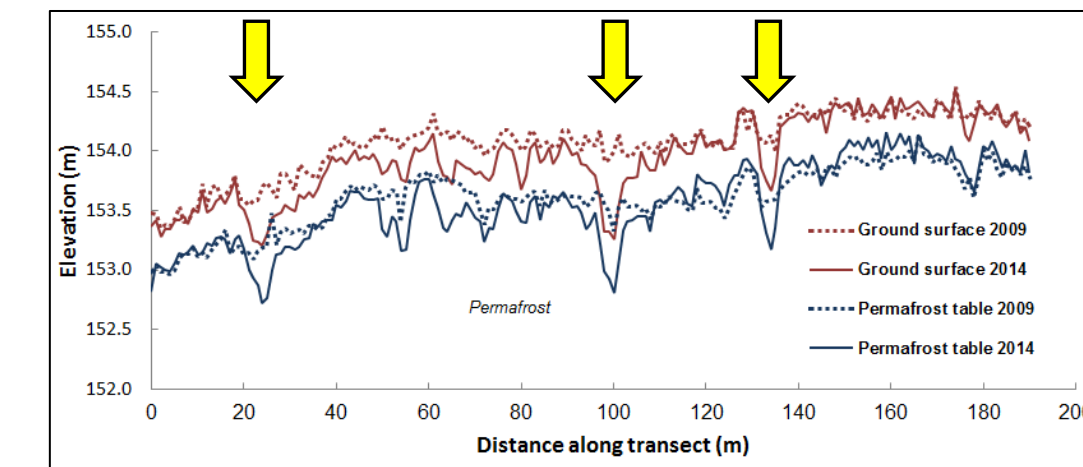


Fig. 10. Yedoma exposure near Umiat showing very large ice wedges underlying residual uplands (see Kanevskiy et al. 2013). These ice bodies developed during the Pleistocene, and are protected from thaw by Holocene peat. Virtually all ice-wedge thermokarst observed thus far involves smaller, overlying ice wedges of Holocene age.

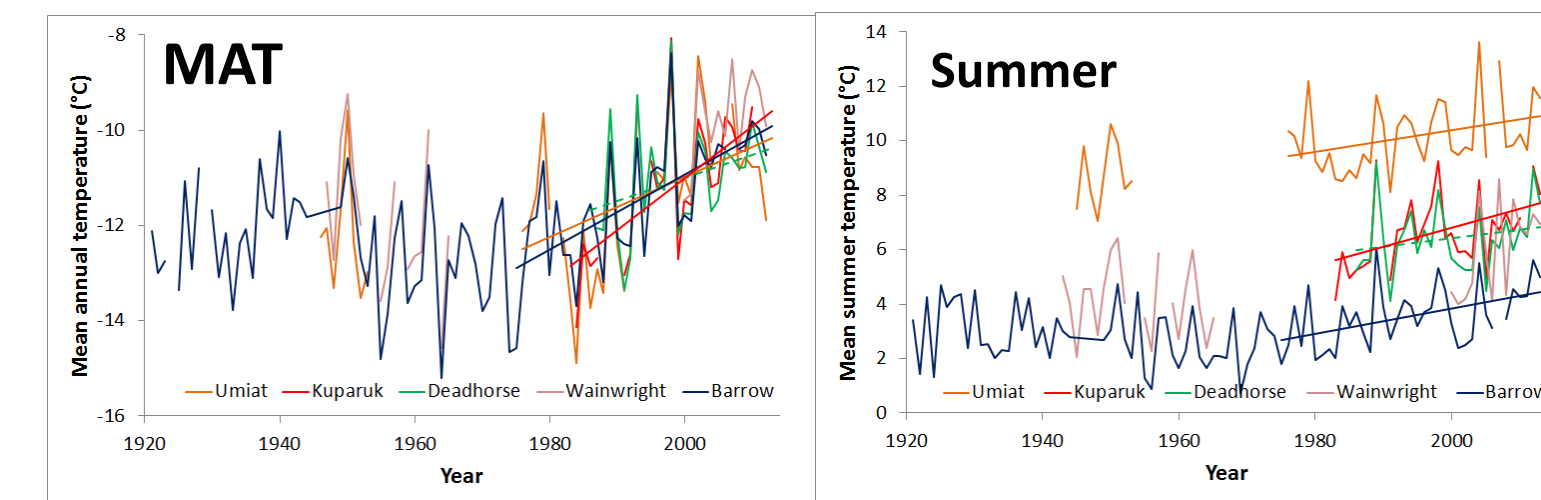


Fig. 11. Climatic drivers of ice-wedge degradation remain under debate. Station data indicate an upward trend in mean annual and mean summer (June–Aug) temperatures since the late 1970s, and there were several exceptionally warm years in the late 1990s and early 2000s. Although there is very little regional variation in MAT across the North Slope, a strong latitudinal climate gradient exists during the summer thaw season.

Conclusions

1. The extent of flooded thermokarst pits increased in residual upland landscapes at 8 of 11 sites (median +10.7%; maximum +134.6%)
2. Initiation of thermokarst first occurred on the western North Slope (before ~1950)
3. Thermokarst pit initiation spread eastward after ~1950; pit formation accelerated after ~1980 on the sand sheet and in foothills yedoma
4. Regional variability in the timing and extent of thermokarst may be partly explained by differences in the physical properties and ice content of surficial materials
5. The strong west-to-east gradient in recent thermokarst rates warrants further investigation and suggests interactions between gradients of summer temperature, winter snowfall, and properties of surficial materials.

Literature Cited

Frost, G V and H E Epstein. 2014. Tall shrub and tree expansion in Siberian tundra ecotones since the 1960s. *Global Change Biology* 20:1264–1277.

Jorgenson, M T, Y L Shur, and E R Pullman. 2006. Abrupt increase in permafrost degradation in Arctic Alaska. *Geophysical Research Letters* 33:L02503.

Jorgenson, M T and J Grunblatt. 2013. Landscape-level ecological mapping of northern Alaska and field site photography. Report for Arctic Landscape Conservation Cooperative, U.S. Fish & Wildlife Service, Fairbanks, AK. 48 pp.

Liljedahl, A K, R P Daanen, G V Frost, N Matveyeva, M Neccsoiu, M K Reynolds, V E Romanovsky and D A Walker. 2013. Observed ice wedge degradation at multiple continuous permafrost locations and their simulated effects on watershed scale hydrology, American Geophysical Union Fall Meeting, C52A-04, December 9-13, San Francisco, CA.

Reynolds M K, Walker D A, Ambrosius K J, Brown J, Everett K R, Kanevskiy M, Kofinas G P, Romanovsky V E, Shur Y, and Webber P J. 2014. Cumulative geoeological effects of 62 years of infrastructure and climate change in ice-rich permafrost landscapes, Prudhoe Bay Oilfield, Alaska. *Global Change Biology* 20:1211–1224.



Acknowledgements

Shell Exploration & Production Company funded this study as part of their multi-year Onshore Environmental Studies Program in northern Alaska.

